Probabilistic Ultra-Wideband TDoA Localization with Bias Correction

Felix Vollmer*, Jan Graßhoff*, Philipp Rostalski*†
*Fraunhofer Institute for Individualized and Cell-Based Medical Technology, Lübeck, Germany
Email: {felix.vollmer, jan.grasshoff, philipp.rostalski}@imte.fraunhofer.de
†Institute for Electrical Engineering in Medicine, University of Lübeck, Lübeck, Germany

***Abstract*—Ultra-wideband (UWB) radio localization is a popular solution for indoor navigation. The time delay of radio signals between agents and anchors enables the inference of the agents' positions. The measurement of the time difference of arrival (TDoA) of these radio signals provides a scalable way to achieve localization. Due to factors like the antenna and room geometry TDoA measurements tend to contain a bias error. We present a probabilistic model-based approach to solve the TDoA localization problem with bias correction. By using stochastic variational Gaussian process (SVGP) regression with a tailored kernel we can exploit the problem structure and efficiently predict the measurement bias. Then we correct this bias by incorporating the Gaussian process (GP) predictions to a factor graph based localization scheme. The method is tested on data recorded from a quadrocopter and validated against an optical marker-based tracking. The framework manages to infer the location of the drone accurately and the proposed bias correction reduces localization errors significantly.**

I. INTRODUCTION

Localization is an important task for many applications. On a large scale satellite navigation like GPS, GLONASS or Galileo is used, which are integrated into most smartphones today. These methods only work outdoors and cannot be used for indoor localization. One popular and low-cost alternative for indoor localization is the use of Ultra-wideband (UWB) transceivers. Especially with the wide availability of cheap transceiver ICs (integrated circuits) for UWB this method gained popularity.

An easily underestimated factor for the range measurements is the antenna design as well as other influences like room geometry. Ledergerber and D'Andrea [1, 2] have shown that the error of the measurements depends on the antenna orientation. Further, they proposed the use of sparse Gaussian processs (GPs) with a periodic kernel to predict this error for two way ranging (TWR) measurements. Zhao *et al.* [3] have demonstrated a correction scheme using neural networks for TWR and time difference of arrival (TDoA) measurements. Further, Li *et al.* [4] presented an effective factor graph based localization scheme for cooperative time of arrival (ToA) measurements.

Building upon previously published bias correction methods, we propose a factor graph based probabilistic localization scheme for TDoA measurements with stochastic variational Gaussian processs (SVGPs) for bias correction and evaluate the novel localization scheme with data from an indoor drone.

II. BACKGROUND

A. Time Difference of Arrival Measurements

The central information we use for localization is the signal propagation time τ between a transmitter and a receiver. Together with a known propagation speed c we get the distance $d = \frac{\tau}{c}$. The propagation speed c is usually well known and therefore we abstract from it in the following. This is the measurement principle employed in ToA measurements. Geometrically speaking it is defined by

$$\hat{d}_{ki} = ||\boldsymbol{x}_k - \boldsymbol{x}_i||_2 \tag{1}$$

where $\boldsymbol{x}_k$ is the position of the receiver and $\boldsymbol{x}_i$ is the position of the transmitter. In practice we usually have to deal with noisy measurements and other uncertainties, so we define $d_{ki} = \hat{d}_{ki} + \epsilon_{ki}$ where ϵ_{ki} is the measurement noise. For ToA measurements we need a reliable and precise clock synchronization to measure the propagation delay between the sender and the receiver. This problem can be mitigated by using TWR, where the signal round-trip time is measured. However, TWR does not scale well for multi-agent systems due to the communication overhead because of the individual communication with every agent.

The measurement of TDoA is less affected by clock synchronization and scales much better than TWR because the agents only need to listen passively. It is geometrically defined by

$$\hat{z}_{ij}^k = \hat{d}_{ki} - \hat{d}_{kj} = ||\boldsymbol{x}_k - \boldsymbol{x}_i||_2 - ||\boldsymbol{x}_k - \boldsymbol{x}_j||_2 \tag{2}$$

where $\boldsymbol{x}_k$ is the receiver and $\boldsymbol{x}_i$, $\boldsymbol{x}_j$ are the transmitters as illustrated in Fig. 1. As TDoA measurements are also noisy, we define them as $z_{ij}^k = \hat{z}_{ij}^k + \epsilon_{ij}^k$ where ϵ_{ij}^k is the noise.

B. Factor Graphs

We use factor graphs to model the problem structure and to solve the inference problem by exploiting the independence statements contained in the graph structure of the model. Even though the history of factor graphs lies in the coding theory [5], the use cases have advanced so that

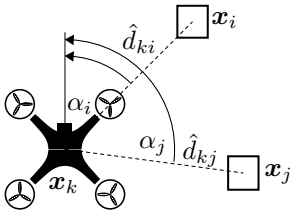

Fig. 1: Top view of the quadrocopter. The TDoA measurement $\hat{z}_{ij}^k$ between agent $\boldsymbol{x}_k$ and the anchors $\boldsymbol{x}_i$ and $\boldsymbol{x}_j$ is the difference of the distances $\hat{d}_{ki}$ and $\hat{d}_{kj}$. The angles α_i and α_j to the anchors depend on the agents orientation and position.

factor graphs, together with the sum-product algorithm, can be seen as a unifying framework for algorithms of a broad variety of domains like optimization, state estimation, sensor fusion, and control systems [6, 7]. Many classical algorithms like the Kalman filter can be seen as a special instance of inference on factor graphs.

Formally a factor graph is described by a factorization $f(S) = \prod_{i=1}^{n} f_i(S_i)$ with the variables $S_i \subseteq S = \{X_1, \ldots, X_m\}$. The factor graph f is an undirected bipartite graph between the functions f_i and the random variables X_j as nodes. In probabilistic settings the variables X_j are typically random variables and the function $f(S)$ describes the joint probability. The marginal distribution of a random variable X_j can be computed by passing messages along the edges of the graph according to the sum-product-rule [8].

We will focus on normally distributed random variables $X \sim \mathcal{N}(\boldsymbol{m}, \Sigma)$ with $W = \Sigma^{-1}$ the information matrix and $\xi = W\boldsymbol{m}$ the weighted mean. Tabulated message passing rules can be derived for various nodes (resp. functions), see [9] for details. In this paper we use Forney style factor graphs where no more nodes than two share a common variable and variables are drawn as an edge between two factor nodes. The equality node serves as a junction point to overcome this restriction. Nodes can be composed to more complex graphs where rules can simply be reused. The graph can also be seen as a tool to develop distributed algorithms by dividing the graph into independent parts and using the opened edges as communication connections [4].

For a given non-loopy graph we can achieve exact inference by passing messages through the graph. For loopy graphs
is not guaranteed to converge but it provides useful results in many practical settings [10].

C. Gaussian processs (GPs)

GPs are widely used nowadays in a variety of applications to solve regression and classification problems. An important advantage of GPs over non-Bayesian machine-learning approaches such as neural networks is, that – as probabilistic models – they are fully compatible with factor graphs. A GP $\varrho(\boldsymbol{x}) \sim \mathcal{GP}(0, k(\boldsymbol{x}, \boldsymbol{x}'))$ with $\boldsymbol{x} \in \mathbb{R}^D$ describes prior knowledge about the distribution of a function $\varrho(\boldsymbol{x})$ and is fully specified by the kernel function $k(\boldsymbol{x}, \boldsymbol{x}')$. By choice of the kernel we can incorporate prior assumptions about the function, e.g. its periodicity or smoothness. Generally, the choice of the right kernel structure is crucial to achieving good performance on a dataset. The kernel usually depends on some free hyperparameters $\boldsymbol{\theta}$, which then are to be optimized on the specific dataset. When the GP is evaluated over a finite set of input points $\{\boldsymbol{x}_1, \ldots, \boldsymbol{x}_n\}$, the function values evaluated at those points have a joint multivariate Gaussian distribution $\big[\varrho(\boldsymbol{x}_1), \ldots, \varrho(\boldsymbol{x}_n)\big] \sim \mathcal{N}(0, K)$ and the kernel matrix K is constructed by evaluation of the kernel function k for all pairs of inputs $\boldsymbol{x}$ and $\boldsymbol{x}'$.

In the standard GP regression setting it is assumed that we have noisy measurements from the latent function ϱ, i.e. we have measured targets $\epsilon_i = \varrho(\boldsymbol{x}_i) + \nu$. In case that the measurement noise is Gaussian white noise $\nu \sim \mathcal{N}(0, \sigma^2)$, there is a closed-form solution for the predictive distribution of function values ϱ_* evaluated at a test-point $\boldsymbol{x}_*$. This so-called posterior itself is a Gaussian distribution given as $\varrho_* \sim \mathcal{N}(\boldsymbol{m}_{\text{post}}, \sigma^2_{\text{post}})$.

For large numbers of samples the prediction via GPs gets computationally expensive due to the inversion of large covariance matrices. SVGPs greatly reduce the computational complexity by using a smaller number of inducing points [11].

The correct selection of the hyperparameters is important to capture the problem structure. By optimizing the marginal likelihood function, the hyperparameters $\boldsymbol{\theta}$ can be optimized. The inducing points for the SVGPs can be seen as additional hyperparameters and be optimized as well.

III. METHODOLOGY

A. Factor Graph Based TDoA Localization

The TDoA measurement equation is inherently nonlinear because of the Euclidean norm. The Euclidean norm for vector $\boldsymbol{a} = [a_1, \ldots, a_n]^T$ is defined by $||\boldsymbol{a}||_2 = \sqrt{\sum_{i=0}^{n} a_i^2}$ and with its gradient $\nabla||\boldsymbol{a}||_2 = \frac{\partial||\boldsymbol{a}||_2}{\partial \boldsymbol{a}} = \frac{\boldsymbol{a}}{||\boldsymbol{a}||_2}$ we can define the linearized Euclidean norm as

$$||\boldsymbol{a}||_{\tilde{2}} = ||\tilde{\boldsymbol{a}}||_2 + \tilde{\boldsymbol{a}}^T/||\tilde{\boldsymbol{a}}||_2 \cdot (\boldsymbol{a} - \tilde{\boldsymbol{a}}) \tag{3}$$

where $\tilde{\boldsymbol{a}}$ is the linearization point of $\boldsymbol{a}$. Now we can linearize $\hat{z}_{ij}^k$ as

$$\hat{z}_{ij}^k \approx ||\boldsymbol{x}_k - \boldsymbol{x}_i||_{\tilde{2}} - ||\boldsymbol{x}_k - \boldsymbol{x}_j||_{\tilde{2}} \tag{4}$$

$$= D + (B_1 - B_2)\boldsymbol{x}_k - B_1\boldsymbol{x}_i + B_2\boldsymbol{x}_j \tag{5}$$

where $B_1 = \frac{\tilde{\boldsymbol{d}}_{ki}^T}{\tilde{d}_{ki}}$, $B_2 = \frac{\tilde{\boldsymbol{d}}_{kj}^T}{\tilde{d}_{kj}}$, $D = \tilde{d}_{ki} - \tilde{d}_{kj} - B_1\tilde{\boldsymbol{d}}_{ki} + B_2\tilde{\boldsymbol{d}}_{kj}$, $\tilde{\boldsymbol{d}}_{ab} = \tilde{\boldsymbol{x}}_a - \tilde{\boldsymbol{x}}_b$ and $\tilde{d}_{ab} = ||\tilde{\boldsymbol{d}}_{ab}||_2$ depend on the linearization points $\tilde{\boldsymbol{x}}_k$, $\tilde{\boldsymbol{x}}_i$ and $\tilde{\boldsymbol{x}}_j$.

With Eq. (5) we can construct the corresponding linearized factor graph in Fig. 2. To infer a new position from a measurement, standard Gaussian message passing over this graph may be used. To do so we have

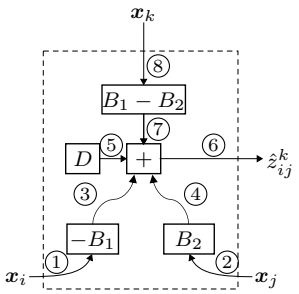

Fig. 2: Factor graph for localization where $\hat{z}_{ij}^k$ is the TDoA distance between agent k and anchors i, j.

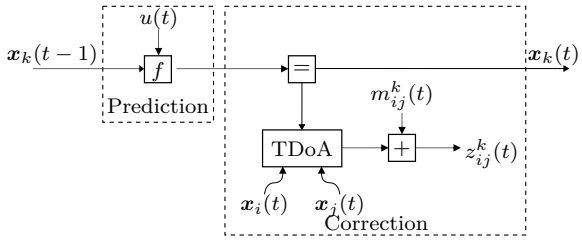

Fig. 3: Integration of the TDoA node from Fig. 2 into the correction step of a Kalman filter slice in factor graph representation. The measurement z_{ij}^k is corrected by the GP prediction m_{ij}^k.

to compute the matrices B_1, B_2 and D based on the current estimate of $\boldsymbol{x}_k$, $\boldsymbol{x}_i$ and $\boldsymbol{x}_j$. Then we compute $\overrightarrow{\mu_3} = \mathcal{N}(-B_1\overrightarrow{\boldsymbol{m}_1}, B_1\overrightarrow{\Sigma_1}B_1^T)$, $\overrightarrow{\mu_4} = \mathcal{N}(B_2\overrightarrow{\boldsymbol{m}_2}, B_2\overrightarrow{\Sigma_2}B_2^T)$ and $\overleftarrow{\mu_7} = \mathcal{N}(\overleftarrow{m_6} - \overrightarrow{m_3} - \overrightarrow{m_4} - D, \overleftarrow{\Sigma_6} + \overrightarrow{\Sigma_3} + \overrightarrow{\Sigma_4})$ with $\overleftarrow{W_7} = \overleftarrow{\Sigma_7}^{-1}$, $\overleftarrow{\xi_7} = \overleftarrow{W_7}\overleftarrow{m_7}$. For the reverse pass through the $B_1 - B_2$ node we compute $\overleftarrow{\xi_8} = B_{12}^T\overleftarrow{\xi_7}$ and $\overleftarrow{W_8} = B_{12}^T\overleftarrow{W_7}B_{12}$ with $B_{12} = B_1 - B_2$.

We can now integrate the TDoA-node from Fig. 2 into the correction step of a full Kalman filter as shown in Fig. 3. The model for the prediction step depends on the application. We use the drone model from Mueller *et al.* [12] for the drone in this setup. It models the drone dynamics and incorporates the gyroscope and accelerometer measurements as input.

Further, we do not have to assume that $\boldsymbol{x}_i$ and $\boldsymbol{x}_j$ are stationary anchors. We can interpret them as other agents and create a bigger distributed Kalman filter (e.g. see Li *et al.* [4]). The structure gets more interconnected then and we can interpret the edges between agents as communication channels, yielding a distributed algorithm.

B. Gaussian Process Error Model

The measurement of UWB based distances has a bias error that strongly correlates with the position and orientation of the agent to the anchors and vice versa [2, 3]. The measurement error is

$$\epsilon_{ij}^k = z_{ij}^k - (||\boldsymbol{x}_k^{\mathrm{gt}} - \boldsymbol{x}_i^{\mathrm{gt}}||_2 - ||\boldsymbol{x}_k^{\mathrm{gt}} - \boldsymbol{x}_j^{\mathrm{gt}}||_2) \tag{6}$$

where $\boldsymbol{x}_i^{\mathrm{gt}}$, $\boldsymbol{x}_j^{\mathrm{gt}}$, $\boldsymbol{x}_k^{\mathrm{gt}}$ are the ground truth positions. For TDoA measurements we have to consider two anchors per measurement and therefore also two orientations. The z angles (yaw angles) are especially relevant because depending on this angle the line of sight between an anchor and the drone may be interrupted (see Section III-C for further details).

We now want to solve the regression problem by predicting the bias using GPs. When we consider angles, a periodic kernel $k_{\mathrm{p}}(r) = \sigma^2 \exp\left(-2\sin(\pi r/T)^2/l^2\right)$ with $T = 2\pi$ the period, l the lengthscale, σ a scaling factor and $r = |\alpha - \alpha'|$ is an obvious choice. As shown in Fig. 1 there are two z angles (α_i and α_j) to the two anchors. For this reason we propose to use the sum

$$\begin{aligned} k_{\mathrm{TDoA_{z1}}}(\alpha_i, \alpha_j, \alpha_i', \alpha_j') = \quad & k_{\mathrm{p}}(|\alpha_i - \alpha_i'|) \\ & + k_{\mathrm{p}}(|\alpha_j - \alpha_j'|) \end{aligned} \tag{7}$$

as a kernel for the bias correction. For comparison, we define the less smooth and non-periodic kernel $k_{\mathrm{TDoA_{z2}}}$ in the same way as the sum of two Matern 5/2 kernels as

$$\begin{aligned} k_{\mathrm{TDoA_{z2}}}(\alpha_i, \alpha_j, \alpha_i', \alpha_j') = \quad & k_{\mathrm{Matern52}}(|\alpha_i - \alpha_i'|) \\ & + k_{\mathrm{Matern52}}(|\alpha_j - \alpha_j'|) \end{aligned} \tag{8}$$

with $k_{\mathrm{Matern52}}(r) = \sigma^2\left(1 + \frac{\sqrt{5}r}{l} + \frac{5r^2}{3l^2}\right)\exp\left(-\frac{\sqrt{5}r}{l}\right)$.

In order to also integrate the remaining rotational angles and the drone position we use the kernel $k_{\mathrm{L}}(\boldsymbol{x}, \boldsymbol{x}') = \theta_0 \exp\left(-\left(1 - \frac{\boldsymbol{x}^T\boldsymbol{x}'}{||\boldsymbol{x}||_2||\boldsymbol{x}'||_2}\right)/\theta_1 - ((||\boldsymbol{x}||_2 - ||\boldsymbol{x}'||_2)^2)/\theta_2\right)$, which was introduced by Ledergerber and D'Andrea [1] for TWR data. The vector $\boldsymbol{x}$ is the position of the anchor from within the drone coordinate system. As before we also apply this kernel to the TDoA problem by using the sum

$$\begin{aligned} k_{\mathrm{TDoA}}(\boldsymbol{x}_{ki}, \boldsymbol{x}_{kj}, \boldsymbol{x}_{ki}', \boldsymbol{x}_{kj}') = \quad & k_{\mathrm{L}}(\boldsymbol{x}_{ki}, \boldsymbol{x}_{ki}') \\ & + k_{\mathrm{L}}(\boldsymbol{x}_{kj}, \boldsymbol{x}_{kj}') \end{aligned}. \tag{9}$$

With these kernels we define the GP models as $\mathcal{GP}(0, k)$. Then we can predict the measurement error ϵ_{ij}^k as the posterior distribution $\epsilon_{ij}^k \sim \mathcal{N}(m_{ij}^k, \sigma_{\mathrm{post}}^2)$ where m_{ij}^k and σ_{post}^2 are the mean and variance of the GP posterior prediction. These predictions are used to correct the measurement inputs of the Kalman filter.

C. Experimental Setup

For the practical experiments a quadrocopter (Crazyflie 2 [13]) was used as an agent to record experimental data. The loco positioning system (lps), with the Decawave DWM1000 chipset, was responsible for UWB communication and localization.

The Crazyflie drone records TDoA measurements from eight anchors that were distributed in the corners of the room. The absolute reference is provided by a Vicon Vero motion tracking system. The drone was tracked with multiple markers to provide position and rotational information, while the anchor positions were tracked with a single marker. The general arrangement of the drone, camera and position system can be seen in Fig. 4.

The TDoA measurements were taken between neighboring anchor id pairs. So for the eight anchors in the setup

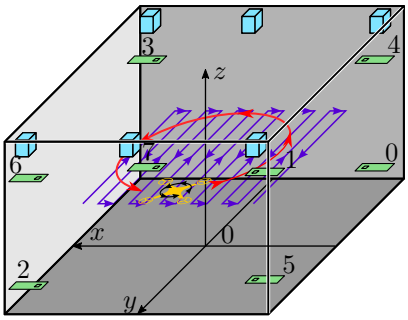

Fig. 4: For the experimental setup a drone (yellow) is flying a trajectory while taking TDoA measurements from the eight anchors (green). A tracking system with six cameras (blue) is used to measure the ground truth positions of both the agent and the anchors. In purple the zigzag training trajectory and in red the circular test trajectory is depicted.

the measurements were taken for the pairs $(0,1)$, $(1,2)$, $\ldots$, $(7,0)$. These measurements were sampled with 180 Hz during the flight and saved on a microSD card together with the accelerometer and gyroscope data. The motion capture system recorded the flight at 300 Hz. The data recorded from the drone and the camera system were synchronized at the take-off point of the drone and the clock drift was compensated.

The quadrocopter is a nonholonomic system, i.e. only the position and the yaw angle can be chosen arbitrarily. The roll and pitch angle depend on the actual flight trajectory. We decided to fly a zigzag and a circle trajectory to capture a wide range of different angles and positions. These trajectories were flown while the quadrocopter rotated around its yaw axis. This way the line of sight between the UWB antenna of the quadrocopter and the anchors gets interrupted depending on the orientation.

The data from the flights was separated into training and test data sets. For a good coverage of the room the zigzag trajectory was used as training data to create the SVGP model for the TDoA measurement error ϵ_{ij}^k. To compute this error, the motion capture system was used as ground truth reference as described in Eq. (6). With this in- and output data the hyperparameters of the GP (including the inducing points) were optimized until convergence. This training was repeated for the kernels with different numbers of inducing points. Then the Kalman filter was run on the uncorrected data and the actual GP input was computed corresponding to Section III-B.

D. Evaluation

To evaluate the effectiveness of the bias correction the localization with the Kalman filter was run twice. Once without any correction of the TDoA measurements and a second time with the SVGP based correction of the measurements. The SVGP model is fed from the estimated state of the Kalman filter.

We define the localization error as the Euclidean norm of the difference between the ground truth reference position

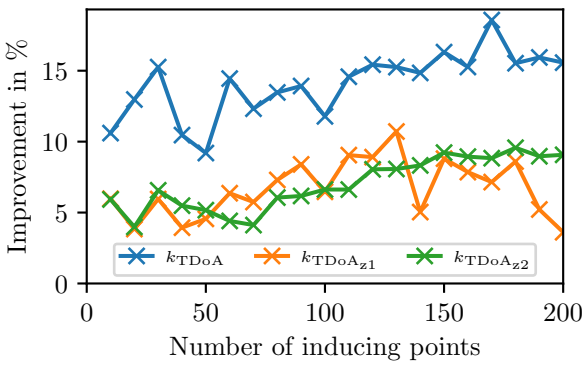

Fig. 5: Improvement of the RMS localization error depends on the number of inducing points and the kernel.

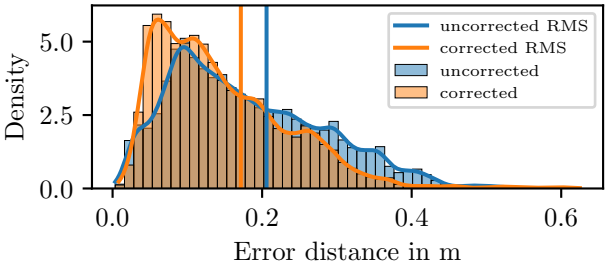

Fig. 6: Comparison between the error distribution of the localization with uncorrected and corrected TDoA measurements. The model was trained with the k_{TDoA} kernel with 30 inducing points on the zigzag pattern and evaluated on a flight with the circular trajectory. There is a significant improvement of the localization error with the GP based bias prediction correction.

of the motion capture camera system and the position of the state vector of the Kalman filter estimation. We evaluate the quadratic mean over these distances.

In Fig. 5 the number of inducing points is evaluated against the improvement of the localization due to the bias correction. A single zigzag flight was used for the training of the bias correction model. The improvement was averaged over three circular test flights. Further, we evaluated the distribution of the localization error. See Fig. 6 for an exemplary distribution.

IV. RESULTS & DISCUSSION

The results of the evaluation show that the probabilistic localization scheme with GP based bias correction can greatly reduce the average localization error. The bias correction model from the zigzag training trajectory is general enough to be transferred to the circle validation trajectory. The improvement correlates with the number of inducing points. Already with 30 inducing points the k_{TDoA}-kernel approach shows very promising results with an improvement of the root mean square (RMS) localization error of 15.25 % with an absolute error of 0.226 m with the uncorrected measurements and 0.192 m with the corrected measurements. Increasing the number of inducing points

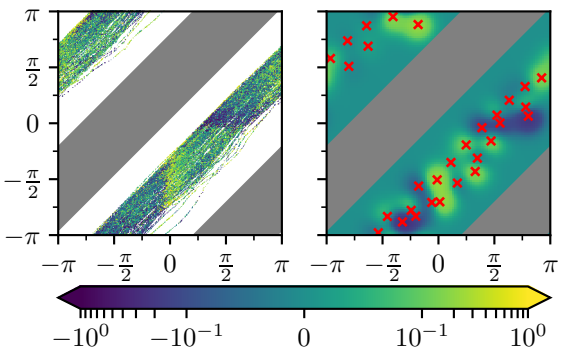

Fig. 7: Left side: Plot of the TDoA measurement errors in m against the z-angles (α_i, α_j) of the agent to an anchor pair (see Fig. 1). Right side: Predicted mean of the sparse GP with the $k_{\mathrm{TDoA}_{z1}}$-kernel, which is supported by the red inducing points. The configuration space is only partly covered because some points lie outside of or too close to the bounding box and cannot be reached due to walls.

leads to further improvement (18.57 % with 170 inducing points).

In Fig. 7 we can see a strong correlation between the measurement error and the drone orientation. The posterior distribution of the GP provides a good model for the error bias. The plot further helps to explain the good result with the rather low number of inducing points. The geometric constraints introduced by the arrangement of the anchors result in an only partially covered input configuration space. Therefore, the GP just has to explain this subspace. Although the figure only shows a representation for the $k_{\mathrm{TDoA}_{z1}}$ kernel, the geometric constraints and thus sparsity also apply to the higher dimensional models with the k_{TDoA} kernel.

Overall the localization improvement increases with the number of inducing points, but with diminishing returns. This is especially true if we take a look at the model complexity because the SVGP model scales with $\mathcal{O}(m^3)$ where m is the number of inducing points. The model convergence depends on the random initialization of the inducing points and therefore the performance graph is slightly noisy. Further, there is no significant difference between the $k_{\mathrm{TDoA}_{z1}}$-kernel and the $k_{\mathrm{TDoA}_{z2}}$-kernel. This can again be explained by the sparse configuration space which provides no real benefit for the periodic kernel.

An interesting extension to the work of Li *et al.* [4] and this work would be the application in multi-agent-systems. The connections of the factor graph between agents would be interpreted as communication and a message passing scheme over the whole graph would cooperatively infer the positions of the multi-agent-system.

References

[1] A. Ledergerber and R. D'Andrea, "Ultra-wideband range measurement model with Gaussian processes," in *2017 IEEE Conference on Control Technology and Applications (CCTA)*, 2017, pp. 1929–1934.

[2] ——, "Calibrating away inaccuracies in ultra wideband range measurements: A maximum likelihood approach," *IEEE Access*, vol. 6, pp. 78 719–78 730, 2018.

[3] W. Zhao, A. Goudar, J. Panerati, and A. P. Schoellig, "Learning-based bias correction for ultra-wideband localization of resource-constrained mobile robots," 2003. arXiv: 2003.09371v1 [cs.RO].

[4] B. Li, N. Wu, H. Wang, P.-H. Tseng, and J. Kuang, "Gaussian message passing-based cooperative localization on factor graph in wireless networks," *Signal Processing*, vol. 111, pp. 1–12, Jun. 2015.

[5] S. M. Aji and R. J. McEliece, "The generalized distributive law," *IEEE Transactions on Information Theory*, vol. 46, no. 2, pp. 325–343, Mar. 2000.

[6] H.-A. Loeliger, J. Dauwels, V. M. Koch, and S. Korl, "Signal processing with factor graphs: Examples," in *First International Symposium on Control, Communications and Signal Processing, 2004.*, IEEE, 2004, pp. 571–574.

[7] C. Hoffmann and P. Rostalski, "Linear optimal control on factor graphs — a message passing perspective —," *IFAC-PapersOnLine*, vol. 50, no. 1, pp. 6314–6319, Jul. 2017.

[8] F. R. Kschischang, B. J. Frey, and H.-A. Loeliger, "Factor graphs and the sum-product algorithm," *IEEE Transactions on Information Theory*, vol. 47, no. 2, pp. 498–519, 2001.

[9] H.-A. Loeliger, J. Dauwels, J. Hu, S. Korl, L. Ping, and F. R. Kschischang, "The factor graph approach to model-based signal processing," *Proceedings of the IEEE*, vol. 95, no. 6, pp. 1295–1322, 2007.

[10] F. R. Kschischang and B. J. Frey, "Iterative decoding of compound codes by probability propagation in graphical models," *IEEE Journal on Selected Areas in Communications*, vol. 16, no. 2, pp. 219–230, 1998.

[11] J. Hensman, N. Fusi, and N. D. Lawrence, "Gaussian processes for big data," in *Uncertainty In Artificial Intelligence, Proceedings of the Twenty-Ninth Conference (2013)*, 2013, pp. 282–290.

[12] M. W. Mueller, M. Hamer, and R. D'Andrea, "Fusing ultra-wideband range measurements with accelerometers and rate gyroscopes for quadrocopter state estimation," in *2015 IEEE International Conference on Robotics and Automation (ICRA)*, May 2015, pp. 1730–1736.

[13] W. Giernacki, M. Skwierczynski, W. Witwicki, P. Wronski, and P. Kozierski, "Crazyflie 2.0 quadrotor as a platform for research and education in robotics and control engineering," in *2017 22nd International Conference on Methods and Models in Automation and Robotics (MMAR)*, IEEE, Aug. 2017, pp. 37–42.